J. Fluid Mech. (1995), *vol.* 290, *pp.* 319–344

Influence of Prandtl number on instability mechanisms and transition in a differentially heated square cavity

By R. J. A. JANSSEN[1] AND R. A. W. M. HENKES[2]

[1] Faculty of Applied Physics, J.M. Burgers Centre for Fluid Mechanics, Delft University of Technology, PO Box 5046, 2600 GA Delft, The Netherlands

[2] Faculty of Aerospace Engineering, J.M. Burgers Centre for Fluid Mechanics, Delft University of Technology, PO Box 5058, 2600 GB Delft, The Netherlands

(Received 6 July 1993 and in revised form 16 September 1994)

The transition from laminar to turbulent of the natural-convection flow inside a square, differentially heated cavity with adiabatic horizontal walls is calculated, using the finite-volume method. The purpose of this study is firstly to determine the dependence of the laminar–turbulent transition on the Prandtl number and secondly to investigate the physical mechanisms responsible for the bifurcations observed. It is found that in the square cavity, for Prandtl numbers between 0.25 and 2.0, the transition occurs through periodic and quasi-periodic flow regimes. One of the bifurcations is related to an instability occurring in a jet-like fluid layer exiting from those corners of the cavity where the vertical boundary layers are turned horizontal. This instability is mainly shear-driven and the visualization of the perturbations shows the occurrence of vorticity concentrations which are very similar to Kelvin–Helmholtz vortices in a plane jet, suggesting that the instability is a Kelvin–Helmholtz-type instability. The other bifurcation for Prandtl numbers between 0.25 and 2.0 occurs in the boundary layers along the vertical walls. It differs however from the related instability in the natural-convection boundary layer along an isolated vertical plate: the instability in the cavity is shear-driven whereas the instability along the vertical plate is mainly buoyancy-driven. For Prandtl numbers between 2.5 and 7.0, it is found that there occurs an immediate transition from the steady to the chaotic flow regime without intermediate regimes. This transition is also caused by instabilities originating and concentrated in the vertical boundary layers.

1. Introduction

The study of natural-convection flows in rectangular cavities, both numerically and experimentally, has received considerable attention in the past few decades. Originally, the motivation for this research came from the many technical and engineering applications. Later, this type of flow, which is recirculating and is characterized by the presence of thin boundary layers along the cavity walls, also became a popular problem to test and compare numerical algorithms that are developed to solve the Navier–Stokes equations. This popularity was expressed by the large number of contributors in a comparison exercise organized by De Vahl Davis & Jones (1983) in which the steady, laminar flow of air in a square, differentially heated cavity with adiabatic horizontal walls was calculated for Rayleigh numbers up to 10^6.

Since then, calculations have been performed for higher Rayleigh numbers and attention has been focused towards describing the temporal behaviour of the flow. This problem was addressed as early as 1980 by Patterson & Imberger who performed a scaling analysis which predicted that, under certain conditions, the approach to steady state (occurring after a sudden increase in the temperature difference between the vertical walls) was oscillatory. The oscillations corresponded to damped internal gravity waves caused by the entrainment of fluid from the intrusions along the horizontal walls by the vertical boundary layers. The decaying oscillatory behaviour was subsequently confirmed by numerical calculations of Patterson & Imberger (1980).

Apart from the approach to steady state, attention has been focused on calculating the transition from laminar to turbulent. Le Quéré & Alziary de Roquefort (1986) calculated the transition to time-periodic flow for air ($Pr = 0.71$) in cavities with aspect ratios (≡ height/width ratios) ranging from 2 to 10. They concluded that the first bifurcation was, for aspect ratios larger than 3, related to the vertical boundary layers becoming unstable. Paolucci & Chenoweth (1989) calculated both bifurcations to periodic and quasi-periodic flow for air in cavities with aspect ratios ranging from 0.5 to 5. For cavities with aspect ratios between 0.5 and 3, they concluded that the first bifurcation is related to an instability occurring in the flow divergence in the horizontal fluid layer near the exit corners, where the vertical boundary layers are turned horizontal by the presence of the horizontal walls. The resulting oscillation was present everywhere in the cavity because of the generation of internal gravity waves. Paolucci & Chenoweth (1989), following a suggestion of Ivey (1984), characterized the flow divergence and the instability as being similar to the hydraulic-jump phenomenon occurring in open channel flows (see e.g. Turner 1973). They characterized this hydraulic jump by defining an internal Froude number. Although the agreement between their calculated Froude numbers and the actual critical Rayleigh numbers calculated for the cavities was good, doubts about the characterization of the instability in terms of the hydraulic-jump mechanism remained. Ravi, Henkes & Hoogendoorn (1994) performed a detailed study of the flow structure in the corner regions where the boundary layers are turned horizontal and concluded that it showed no characteristics of an internal hydraulic jump, but that the flow separation was instead caused by a thermal mechanism. The second instability, as calculated by Paolucci & Chenoweth (1989) was caused by an instability occurring in the vertical boundary layers. The frequencies obtained by them were largely in agreement with the results obtained by Henkes (1990) and showed close agreement with the results of Gill & Davey (1969) for the instability occurring in the natural-convection boundary layer along an isolated vertical plate.

All these studies were concerned with air as the working fluid. In addition water ($Pr = 7.0$) has received some attention. Schladow, Patterson & Street (1989), Schladow (1990) and Patterson & Armfield (1992) considered the *transient* instabilities that occur in a square cavity filled with water immediately after a temperature difference is imposed. These studies, however, are not concerned with calculating the transition to an unsteady flow regime. Henkes (1990) performed some calculations for water to find the transition to unsteady flow. He obtained high frequencies in the unsteady solution, probably related to the boundary-layer instability, but could not obtain results that were (fully) grid-independent. Also, the critical Rayleigh number in the square cavity was several orders of magnitude larger than could be expected on the basis of the results of Gill & Davey (1969) for the isolated plate, casting doubts on the previously assumed analogy.

These previous studies were mostly numerical studies in which the full, time-

dependent Navier–Stokes equations were integrated and the solution for large time was calculated. Another approach which may be used to determine the transition to unsteady flow numerically has been employed by Winters (1987, 1988, 1989). In this approach, a relatively modern computational technique is used for locating the oscillatory instability by assuming that the bifurcation is a Hopf bifurcation and by employing an *extended* system of *steady* equations whose solution yields the critical parameter values at the bifurcation point. Compared to direct simulations of the full time-dependent Navier–Stokes equations, this approach has the advantages of a much higher accuracy in determining the bifurcation point and of being able to trace unstable as well as stable solutions. The main disadvantage is the inability to study flows with a complex time-dependence.

The present study addresses the questions concerning the instability mechanisms for the two instabilities in the square cavity with adiabatic horizontal walls as mentioned above. This is accomplished by solving the time-dependent Navier–Stokes equations and by investigating the relationship between the Prandtl number and the different instabilities with their resulting oscillations in the solution for large time of the cavity flow. Detailed calculations were performed for the square cavity for Prandtl numbers ranging from 0.25 to 7.0. Since it was found that the boundary-layer-type instability was not much influenced by the aspect ratio, some calculations were also performed for an aspect ratio 4. The frequencies are determined from power spectra using typically some 10000 time steps to calculate a single power spectrum. Whereas the periodic and quasi-periodic flow regimes are characterized by a single sharp spike and two sharp spikes in the power spectrum respectively (plus spikes corresponding to linear combinations of the fundamental frequencies), for higher Rayleigh numbers the spectra broaden and the (relative) magnitude of the spikes diminishes, suggesting that a chaotic regime has been reached. The results in the square cavity indicate that the transition from laminar to chaotic flow for $Pr \leqslant 2.0$ is through periodic and quasi-periodic flow regimes. The calculations show strong evidence that the instability occurring in the fluid layer exiting from the corners where the vertical boundary layers are turned horizontal is basically a Kelvin–Helmholtz-type instability and that it is related to the instability occurring in a plane jet which has inflexion points in its velocity distribution. It is not related to a hydraulic jump. The results also show that the instability originating in the vertical boundary layers of the cavity is indeed related to the instability in the natural-convection boundary layer along the vertical plate. However, the instability in the cavity turns out to be strongly shear-driven (i.e. mechanically driven) which is different from the instability along the isolated vertical plate which is mainly buoyancy-driven. This can also explain the large discrepancy in critical Rayleigh numbers which is observed between the cavity and the plate configurations.

2. Mathematical description

2.1. *Flow equations*

Consider a two-dimensional rectangular cavity with height H and width L and with isothermal vertical sidewalls. The left wall is held at a fixed temperature T_h and the right wall at a temperature T_c ($T_h > T_c$). The horizontal top and bottom walls are considered to be perfectly adiabatic. The gravitation g acts in the negative x_2-direction (see figure 1).

The flow in the square cavity is fully described by the two-dimensional Navier–

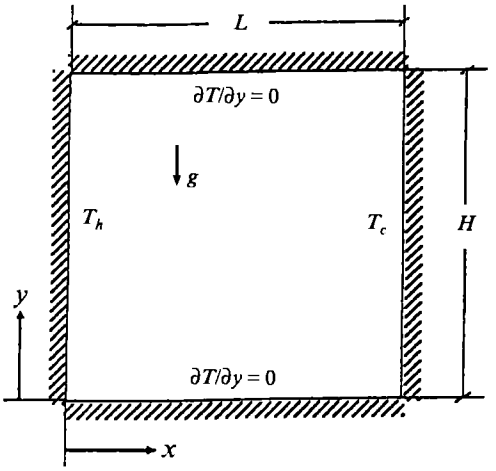

FIGURE 1. The geometry under consideration.

Stokes equations. Under the Boussinesq approximation, these equations read:

$$\left.\begin{aligned} \frac{\partial u_i}{\partial x_i} &= 0, \\ \frac{\partial u_i}{\partial t} + u_j\frac{\partial u_i}{\partial x_j} &= -\frac{1}{\rho}\frac{\partial p}{\partial x_i} + g\beta(T - T_0)\delta_{i2} + \nu\frac{\partial^2 u_i}{\partial x_j^2}, \\ \frac{\partial T}{\partial t} + u_j\frac{\partial T}{\partial x_j} &= a\frac{\partial^2 T}{\partial x_j^2}. \end{aligned}\right\} \tag{2.1}$$

Here, the summation convention has been used: in every term, a summation has been performed from 1 to 2 over repeated indices. In equations (2.1), u_i denotes the velocity component in the x_i-direction, ρ is the density, p is the pressure, ν is the kinematic viscosity, β is the coefficient of thermal expansion, T is the temperature, T_0 is a reference temperature and a the thermal diffusivity. For ease of notation, in the following, u_1 and u_2 will be denoted as u and v respectively and x_1 and x_2 will be denoted as x and y respectively.

These equations can be made dimensionless using the length scale H, the time scale $H/(g\beta\Delta T H)^{1/2}$, the temperature scale $T_0 = T_c$ and the temperature difference $\Delta T = T_h - T_c$. For the velocity scale we take the buoyant scale $(g\beta\Delta T H)^{1/2}$. This leads to a set of non-dimensionalized equations, governed by only three characteristic numbers: the Rayleigh number $Ra = g\beta\Delta T H^3/(\nu a)$, the Prandtl number $Pr = \nu/a$ and the aspect ratio $A = H/L$.

To fully specify the mathematical problem both boundary and initial conditions have to be specified. The boundary conditions used in the present study are

$$\left.\begin{aligned} u &= v = 0, && x = 0, L, \quad y = 0, H, \\ T &= T_h, && x = 0, \\ T &= T_c, && x = L, \\ \partial T/\partial y &= 0, && y = 0, H. \end{aligned}\right\} \tag{2.2}$$

As initial condition we take fields calculated earlier for a different Rayleigh number

and/or a different Prandtl number. If a different number of grid cells is used, the fields are interpolated to the new grid using linear interpolation.

2.2. *Energy balance*

In principle, the Navier–Stokes equations, as presented in the previous subsection, completely describe the mathematical problem (in conjunction with properly specified boundary and initial conditions). It is, however, instructive to consider the kinetic energy for which the conservation equation can be derived from the Navier–Stokes equations. To derive the equation describing the conservation of *fluctuating* kinetic energy, we first perform the Reynolds decomposition into a mean and a fluctuating quantity. For a scalar variable $\phi(x_i, t)$, this means

$$\phi(x_i, t) = \overline{\phi}(x_i) + \phi'(x_i, t) \quad \text{with} \quad \overline{\phi}(x_i) = \lim_{t^* \to \infty} \frac{1}{t^*} \int_{-t^*/2}^{t^*/2} \phi(x_i, t) \mathrm{d}t. \tag{2.3}$$

The equation describing the conservation of fluctuating kinetic energy, $u_i' u_i'/2$, can be derived from the momentum equation in the Navier–Stokes equations. First, the momentum equation is multiplied by u_i after which the decomposition is introduced in the resulting equation. From this equation, the original momentum equation multiplied by $\overline{u}_i$ is subtracted. This results in an equation describing the conservation of fluctuating kinetic energy, which reads

$$\begin{aligned} \frac{\partial u_i' u_i'/2}{\partial t} = & \underbrace{-\frac{\partial}{\partial x_j}\left(u_i' \overline{u}_j\, \overline{u}_i + u_j u_i' u_i'/2 + u_j' p/\rho + \nu u_i' \frac{\partial u_i}{\partial x_j}\right)}_{\text{I}} \\ & \underbrace{+ \overline{u}_i\, \overline{u}_j \frac{\partial u_i'}{\partial x_j} - \nu \frac{\partial \overline{u}_i}{\partial x_j} \frac{\partial u_i'}{\partial x_j} + g\beta u_i' (\overline{T} - T_0)\delta_{i2}}_{\text{II}} \\ & \underbrace{-u_i' u_j' \frac{\partial \overline{u}_i}{\partial x_j} - \nu \left(\frac{\partial u_i'}{\partial x_j}\right)^2 + g\beta u_i' T' \delta_{i2}}_{\text{III}}. \end{aligned} \tag{2.4}$$

Here, the first group of terms on the right-hand side (denoted by I) is a divergence. Integrating equation (2.4) over the entire cavity, employing Gauss' divergence theorem and the fact that all fluctuating velocity components at all cavity walls are zero, shows that the terms in group I do not contribute to the total fluctuating kinetic energy. This group can be interpreted as representing transport of fluctuating kinetic energy. The second group, denoted by II, contains terms that are all *linear* in the fluctuating velocity components. Reynolds-averaging of equation (2.4) would make the terms in this group zero (for a periodic oscillation in the flow, taking an average over one period of the oscillation suffices to make the terms in group II equal to zero). Group III contains terms which neither by integration in space nor by integration in time can be made equal to zero. These terms describe production and dissipation of fluctuating kinetic energy. The term $-u_i' u_j' \partial \overline{u}_i/\partial x_j$ describes the production of fluctuating kinetic energy by the shear of the mean flow, $g\beta u_i' T' \delta_{i2}$ describes the production of fluctuating kinetic energy by buoyancy forces and $-\nu(\partial u_i'/\partial x_j)^2$ describes the viscous dissipation of fluctuating kinetic energy.

3. Numerical treatment

The equations (2.1) are discretized by the finite-volume method, employing a staggered grid. The integration in time is performed fully implicitly: all spatial derivatives are evaluated at the new time level. The unsteady term, the fluxes through the sides of the finite volumes and the source are further discretized with finite differences. The unsteady term is discretized with three time levels, giving a second-order truncation error in time. The diffusion part of the flux is discretized with a second-order truncation error, whereas the convection is discretized with a fourth-order-accurate approximation for the convective derivative. More details about the discretization can be found in Janssen & Henkes (1993).

The grid is constructed by firstly distributing the velocity grid lines according to a stretching function. This distribution is such that the boundaries of the physical domain coincide with velocity grid lines. Secondly, the scalar points are placed precisely in the centre of the scalar volumes. For the u-velocities, the stretching function is chosen as

$$\frac{x_i}{L} = \frac{i}{i_{max}} - \frac{1}{2\pi}\sin(2\pi\frac{i}{i_{max}}) \quad i = 0, 1, \ldots, i_{max}. \tag{3.1}$$

The same function is used for the v-velocities. This distribution concentrates grid points in the boundary layers along the walls.

As an implicit method is used to discretize the time-dependent equations, at each new time level a system of nonlinear equations has to be solved. The solving of the different equations is decoupled, the equations are linearized by evaluating all nonlinearities at the previous iteration level and the discrete systems belonging to each of the equations are iteratively solved using a line Gauss–Seidel method. Sweeps are made through the computational domain from $i = 0$ to $i = i_{max}$ and vice versa. After each sweep the pressure is calculated from a pressure-correction equation. At the walls, a zero gradient for the pressure correction is prescribed. To solve the discretized Poisson equation for the pressure correction, the preconditioned conjugate gradient ((M)ICCG) method was used, in which a (Modified) Incomplete Cholesky decomposition of the band matrix, that results from the discretization of the Poisson equation, was used as a preconditioning for the Conjugate Gradient (CG) algorithm. More details about the (M)ICCG-algorithm can be found in Meijerink & Van der Vorst (1977) and Van der Vorst (1989).

4. Known structures

4.1. *Basic flow structures*

If the Rayleigh number is increased to infinity, certain terms in the Navier–Stokes equations may be neglected and the flow is then described by an asymptotic description. Considerable effort has been spent in the past both theoretically (Elder 1965; Gill 1966; Graebel 1981) and numerically (Blythe, Daniels & Simpkins 1983; Henkes & Hoogendoorn 1993) to determine these asymptotic structures. In spite of this, however, only an incomplete picture of the asymptotic structures in the cavity flow is presently available. The calculations performed by Henkes & Hoogendoorn (1993) are the most relevant for the present study since approximately the same range of Prandtl numbers is considered. They numerically solved the Navier–Stokes equations for increasing Rayleigh number, and they derived the high-Rayleigh-number scalings from the results. These calculations show that the flow follows different Rayleigh-number scalings in the vertical boundary layers along the isothermal cavity walls, the

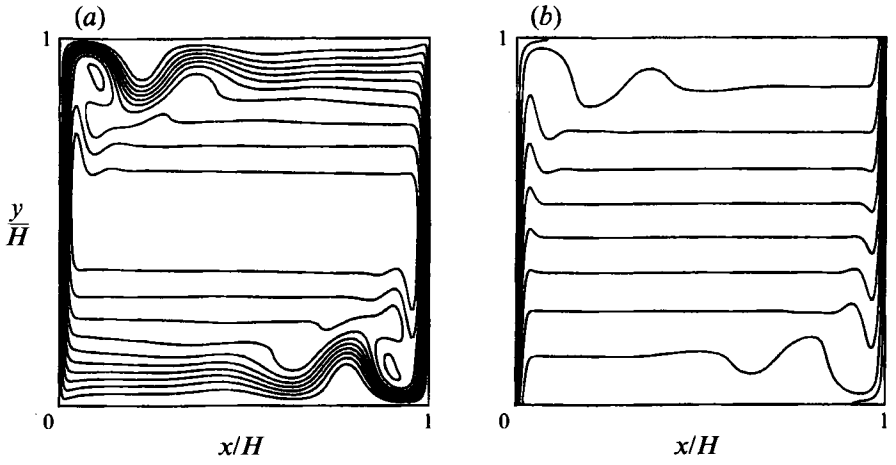

FIGURE 2. Flow field for the steady flow of air ($Pr = 0.71$) at $Ra = 10^8$; (*a*) streamlines, (*b*) isotherms. Contour lines correspond to 10 equidistant values.

horizontal boundary layers along the adiabatic cavity walls, the corner regions where the vertical boundary layers are turned horizontal and the core region. Thus, these calculations indicate that there are at least four different composite asymptotic structures in the cavity flow. More analysis is required to detect whether a structure can be further split up in asymptotic layers. In particular the asymptotics in the corner seem to be complicated, and are expected to be described by multiple asymptotic layers.

For the large values of the Rayleigh number considered in this paper (of the order of $10^8 - 10^{10}$) these four structures are already clearly distinguishable in the flow as is shown in figure 2, in which both the streamlines and the isotherms in the square cavity for air ($Pr = 0.71$) at a Rayleigh number of 10^8 are depicted. Two of the regions are of special importance in this investigation: the core region and the vertical boundary layers. The core can be considered to be an inviscid, stably stratified medium with an approximately constant stratification (which is clearly visible in figure 2*b*). As can be seen in figure 2(*a*), the streamlines in the core are (almost) horizontal and the flow is (almost) parallel. The vertical boundary layers, on the other hand, resemble the natural-convection boundary layers along isothermal vertical plates in a stratified environment.

What is also clearly visible in figure 2(*a*), is the occurrence of a recirculation region and a flow divergence in the upper left and lower right corners of the cavity. Ravi *et al.* (1994) have studied the origin of the recirculation region and the flow divergence and found that they were caused by a thermal mechanism which is related to the temperature stratification in the core region of the cavity. It has been found in their calculations that these structures are very much dependent on the Prandtl number: the recirculation region in the steady flow vanishes for Prandtl numbers larger than 1.4 and the flow divergence for Prandtl numbers larger than 2.0.

4.2. *Internal gravity waves*

A medium that is continuously and stably stratified, as for instance the core region in the square cavity, allows internal gravity waves to occur. For standing internal gravity waves in an inviscid, continuously stratified medium, Thorpe (1968) calculated wave profiles and eigenfrequencies of the oscillations. He expanded the solution of the flow equations in a series expansion, the convergence of which depended on the wave

amplitude being small. To first order, assuming the temperature stratification S ($\equiv (H/\Delta T)\,\partial T/\partial y$) and thus the density stratification to be constant, the eigenfrequencies are given by

$$\frac{fH}{(g\beta\Delta TH)^{1/2}} = \frac{1}{2\pi}\left(S\,\frac{\alpha_x^2}{\alpha_x^2+\alpha_y^2}\right)^{1/2}. \tag{4.1}$$

Here, α_x and α_y denote wavenumbers in the x- and y-directions respectively. Equation (4.1) can also be derived directly from the Taylor–Goldstein equation, describing the linear stability of an inviscid, stratified parallel flow, assuming the base flow velocity to be constant (see Drazin & Reid 1981). If standing waves are considered, $L\alpha_x/\pi$ and $H\alpha_y/\pi$ take integer values only. However, as emphasized by Turner (1973), equation (4.1) also gives the frequency of travelling internal gravity waves (at least those of small amplitude). These travelling waves occur particularly if there is a localized source of energy, the waves then travelling away from the edges of the source.

Two important properties of these travelling gravity waves are reflected in equation (4.1). Firstly, since α_x and α_y are wavenumbers, they describe the direction in which a wave travels. Waves of a given frequency f travel under a fixed angle θ to the horizontal, irrespective of their wavelength. Here, θ is given by

$$\cos\theta = \frac{2\pi}{S^{1/2}}\frac{fH}{(g\beta\Delta TH)^{1/2}}. \tag{4.2}$$

Secondly, since $\alpha_x^2/(\alpha_x^2+\alpha_y^2) \leqslant 1$, no oscillations with a frequency $fH/(g\beta\Delta TH)^{1/2}$ larger than $S^{1/2}/2\pi$ are possible in the core region. This frequency $S^{1/2}/2\pi$ is known as the Brunt–Väisälä frequency.

4.3. *Boundary-layer instability*

The boundary layers along the isothermal, vertical walls of the cavity resemble those along an isolated, heated vertical plate. The stability of these boundary layers has long been a subject of investigation and several experimental and numerical studies on the boundary layers along an isolated vertical plate have been performed, mainly for air and water. As is well-known from these studies, travelling waves can occur in these boundary layers. For *forced*-convection boundary layers, such travelling waves are called Tollmien–Schlichting waves.

The numerical investigations of instabilities in the boundary layer have been performed using linear stability analyses. Nachtsheim (1963) performed such a study for the boundary layer along a semi-infinite, vertical, hot plate placed in an isothermal environment. However, in the rectangular cavity there is the presence of the adiabatic horizontal walls and, apart from effects in the corners where the flow is turned horizontal, the main consequence of this presence of the horizontal walls is the appearance of the stable stratification in the core region of the cavity. Hence, the boundary layer is placed in a stratified environment and not in an isothermal one. Gill & Davey (1969) performed a linear stability analysis of the natural-convection boundary layer along the vertical plate, placed in a stably stratified environment. In their study, a detailed analysis of the Prandtl-number dependence of the linear boundary-layer instability was also performed. However, in their configuration the plate temperature also increased linearly with height, whereas the cavity wall is isothermal. Also, Gill & Davey (1969) assumed the steady base flow to be parallel and it therefore does not describe the development of the boundary layer in the lower part of the cavity.

These linear stability analyses predict the critical Rayleigh number at which the flow first becomes unstable. They do not predict a single frequency but a range of frequencies to appear in the solution. As noted by Gebhart *et al.* (1988), both for an isothermal flat plate and for a plate with a constant heat flux placed in an isothermal environment, the boundary layer along the plate has a strong filtering effect, in which only a narrow band of frequencies is strongly amplified. Basically, this results in essentially a single frequency becoming dominant. This frequency, scaled with $(g\beta\Delta T)^{2/3}\nu^{-1/3}$ is independent of the position along the plate and Gebhart & Mahajan (1975) denote this frequency as the 'characteristic frequency' of the boundary layer.

We will compare frequencies and critical Rayleigh numbers obtained for the rectangular cavity heated from the side with results obtained by Gill & Davey (1969) for the boundary layer along the flat plate for different Prandtl numbers. Gill & Davey (1969) present their results in terms of a critical Reynolds number R_{GD} and a dimensionless wavenumber α_{GD} and wave speed c_{GD}. The transformations to the 'characteristic' dimensionless frequency of the boundary layer and to the critical Rayleigh number used in the present study are

$$\frac{f\nu^{1/3}}{(g\beta\Delta T)^{2/3}} = 2^{-4/3}R_{GD}^{1/3}\ \frac{\alpha_{GD}c_{GD}}{2\pi}, \tag{4.3}$$

$$Ra_{cr} = 4(R_{GD}\ Pr)^4 S^3. \tag{4.4}$$

Here, the critical Rayleigh number and the frequency $f\nu^{1/3}/(g\beta\Delta T)^{2/3}$ are based on $2(T_h - T_\infty)$ where T_∞ denotes the temperature infinitely far away from the plate. This has been done to make a meaningful comparison with the cavity geometry possible. Replacing T_∞ by $(T_h + T_c)/2$ gives $\Delta T = T_h - T_c$, the definition introduced earlier.

5. Results

In this section, the results obtained in this study will be presented together with a discussion of these results both in terms of the transition of the laminar flow to a chaotic flow and in terms of instability mechanisms responsible for the observed bifurcations in the flow. In all cases considered, we study the transition from laminar to chaotic flow for a fixed Prandtl number by changing the Rayleigh number.

5.1. *Transition*

The results in the square cavity can, as far as the transition is concerned, be classified into two major groups: those for Prandtl numbers less than or equal to 2 and those for Prandtl numbers greater than or equal to 2.5.

For Prandtl numbers between 0.25 and 2.0, calculations were performed mainly using a grid with 160×160 grid cells. By time-step refinement, it was checked that a time step $\Delta t(g\beta\Delta T H)^{1/2}/H = 1/32$ gave almost time-step-independent results. To study the grid-dependence of the obtained results, calculated frequencies for the oscillation in the flow for $Pr = 0.25$ at $Ra = 4.25 \times 10^7$ have been tabulated in table 1. Clearly, the frequency is almost grid-independent on the 160×160 grid.

To look for oscillations occurring somewhere in the cavity, several characteristic quantities, which are located in different regions of the cavity, are monitored. Apart from a monitor point located in the upper part of the boundary layer along the hot wall, the monitored quantities are v_{max}, the maximum of the vertical velocity along

Grid	$\frac{fH}{(g\beta\Delta TH)^{1/2}}$
40 × 40	0.113
80 × 80	0.121
160 × 160	0.123

TABLE 1. Results for the frequency of the instability in the flow at $Ra = 4.25 \times 10^7$ and $Pr = 0.25$ on different grids.

the horizontal line at the cavity midheight; u_{max}, the maximum of the horizontal velocity along the vertical line at half the cavity width; and S, the stratification in the centre of the cavity. It should be stressed that the calculated power spectra depend on the location inside the cavity, where the monitored quantity is being observed. Not just the relative magnitude of the spikes can vary from place to place but it is also possible that a certain frequency is not present at all in the power spectrum of one of the monitored quantities. This necessitates the use of monitor quantities which are spread over the different regions inside the cavity.

The transition from laminar to chaotic flow, for Prandtl numbers between 0.25 and 2.0, takes place in agreement with the scenario presented by Ruelle & Takens (1971). The flow first bifurcates at a certain critical Rayleigh number Ra_{cr1} from steady to time-periodic. The time-periodic flow is characterized by the fact that the power spectra of monitored quantities show a spike at a single frequency and (owing to nonlinear self-interaction, see Drazin & Reid 1981) its higher harmonics. Then, at a higher Rayleigh number, Ra_{cr2}, a subsequent bifurcation takes place from periodic to quasi-periodic flow (characterized by a power spectrum with spikes at two fundamental frequencies plus spikes at linear combinations of these fundamental frequencies). At even higher Rayleigh numbers, the power spectra undergo a further change: the spikes broaden and their (relative) magnitude diminishes, suggesting that a chaotic flow regime has been reached. In any event, the spectra of the monitored quantities can no longer be described as a linear combination of a small number of discrete frequencies. Power spectra showing this trend have been depicted in figure 3(*a–f*). This figure shows both time series and power spectral density functions for the calculated temperature at the monitor point, located in the upper part of the left vertical boundary layer, at $(x/H, y/H)=(0.0025,0.90)$. The Prandtl number was 0.71 (corresponding to air) and the Rayleigh numbers are 2×10^8 (*a,b*: periodic flow regime), 3×10^8 (*c,d*: quasi-periodic flow regime) and 7.5×10^8 (*e,f*: chaotic flow regime).

The two fundamental frequencies that were obtained for the different Prandtl numbers in the transition range could be divided into two classes: a lower one (for which $fH/(g\beta\Delta TH)^{1/2}$ is in the range 0.05–0.12) and a higher one ($fH/(g\beta\Delta TH)^{1/2}$ in the range 0.5–0.7). The lower frequency was found in all monitored quantities whereas the higher frequency was only apparent in the downstream part of the vertical boundary layers. This is due to the fact that the lower frequency was below the Brunt–Väisälä cut-off frequency of the core region and, hence, internal gravity waves with this frequency could be sustained in the interior of the cavity. These waves are shown in figure 4, in which the temperature perturbations in the cavity are depicted, i.e. the time-averaged temperature at every grid point is subtracted from the instantaneous temperature value at a certain time-instant. The animation shows that the waves travel under the angle θ, given by equation (4.2), and that they travel from

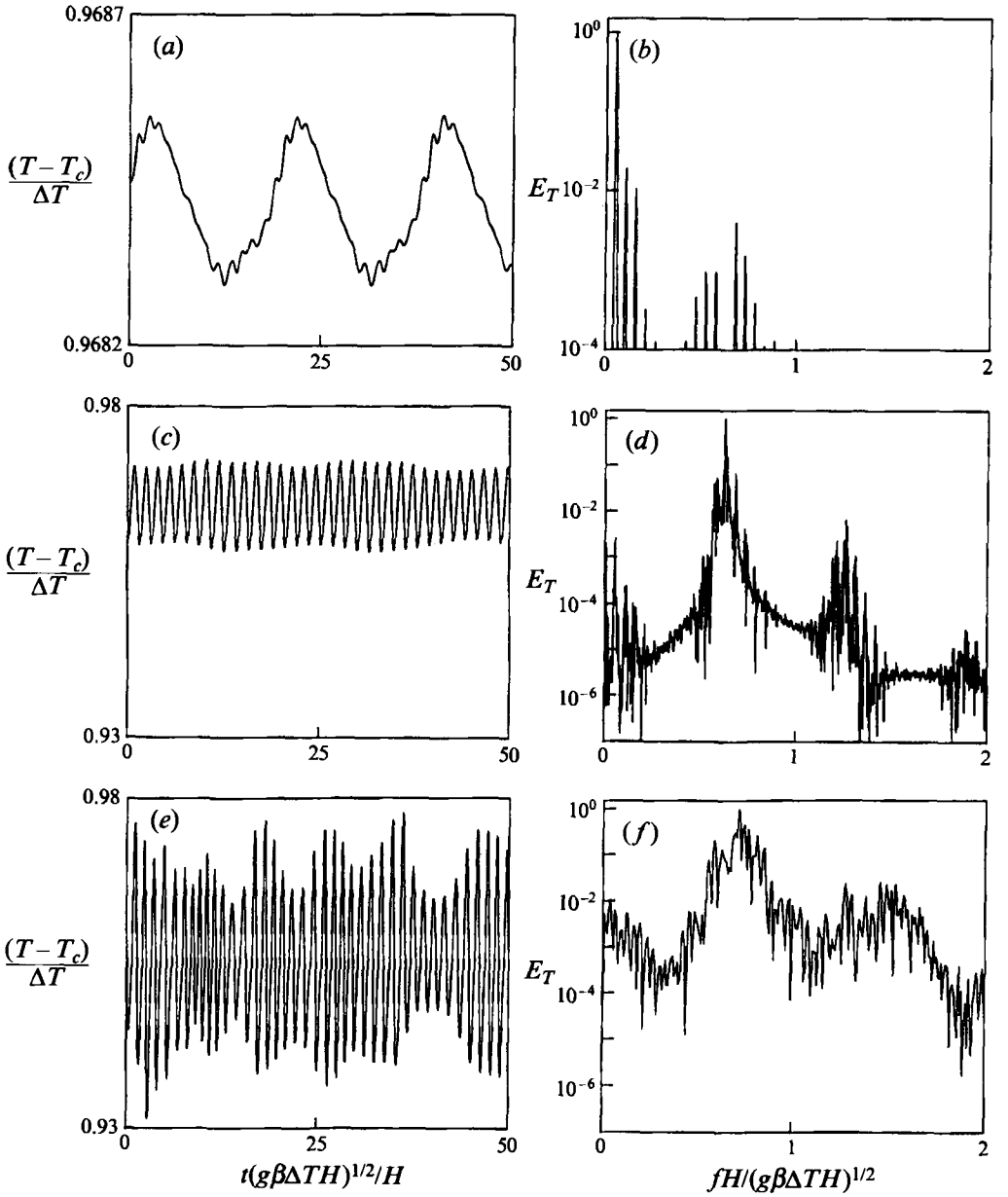

FIGURE 3. Time series (a, c, e) and corresponding power spectra (b, d, f) of the temperature at the monitor point $(x/H, y/H)$=(0.0025,0.90) for air in the square cavity. For the purpose of normalization, the power spectra have been divided by the largest value. (a, b) $Ra = 2 \times 10^8$, (c, d) $Ra = 3 \times 10^8$, (e, f) $Ra = 7.5 \times 10^8$.

the centre towards the upper right and lower left corners of the cavity. The higher frequency was above the cut-off frequency and, hence, no internal waves could be generated with this frequency, confining it to the vertical boundary layers.

For Prandtl numbers in the range 2.5–7.0, no such conclusions about the transition could be drawn from the results of the calculations. Instead, there was an immediate bifurcation from the steady to the chaotic flow regime. This is illustrated by the

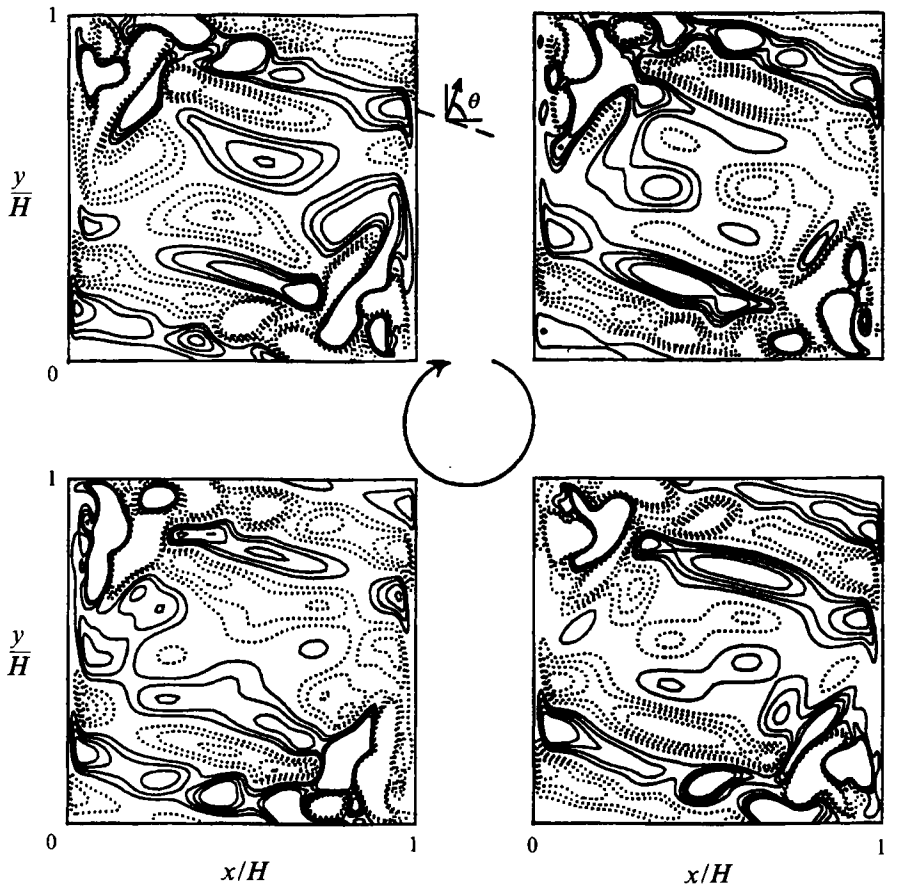

FIGURE 4. Internal waves in the square cavity, corresponding to fluctuations in the temperature for air at $Ra = 2 \times 10^8$. The dotted contour lines correspond to negative values. Contour lines correspond to ± 0.0005, ± 0.001, ± 0.0015 and $\pm 0.002\ \Delta T$.

results for $Pr = 4$ on the 160×160 grid. For $Ra = 2.50 \times 10^{10}$, the solution for large time was steady. An increase in the Rayleigh number to 2.51×10^{10} causes the flow to become time-dependent, as can be seen in figures 5(*a*) and 5(*b*). Figure 5(*a*) shows the final calculated part of the time-evolution of the temperature of the monitor point $(x/H, y/H)$=(0.004,0.90) at $Ra = 2.51 \times 10^{10}$, whereas figure 5(*b*) shows the corresponding power spectrum. Clearly, the power spectrum has broadband characteristics and no true dominant peaks, especially when comparing it with the spectra obtained for *air* in the transitional regime (see figures 3*b* and 3*d*). Also, the fact that such a small increase in the Rayleigh number causes such a large difference in the solution for large time of the flow supports the assumption that there is an immediate transition from steady to chaotic without intermediate periodic and/or quasi-periodic flow regimes. For none of the Prandtl numbers investigated in the range 2.5–7.0, could a periodic or quasi-periodic flow regime be established for any of the calculated Rayleigh numbers. The dominant part of the power spectra was in all instances in the range 0.80–1.0 (in units of $(g\beta\Delta T H)^{1/2}/H$) and the oscillations were strongest in the downstream parts of the vertical boundary layers. This suggests that the transition for these Prandtl numbers is related to a boundary-layer-type instability.

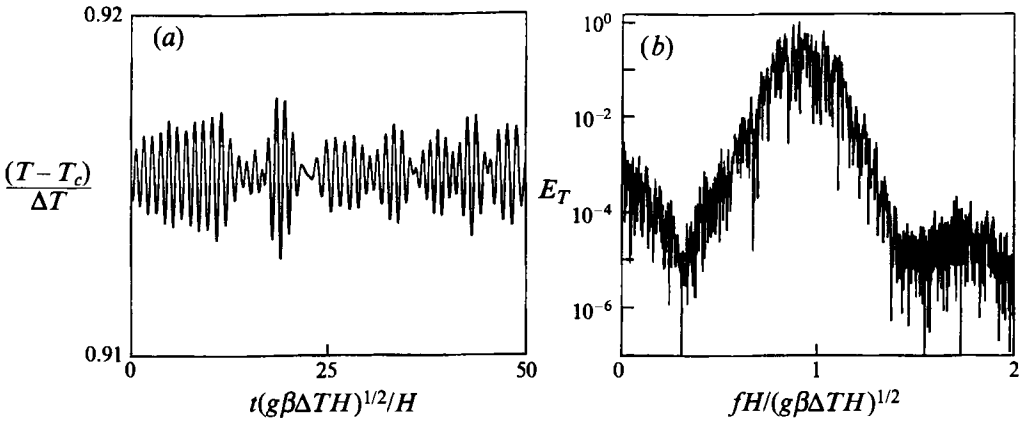

FIGURE 5. Time series and (normalized) power spectrum of the temperature oscillation at the monitor point $(x/H, y/H)$=(0.004,0.90) for $Pr = 4$ on the 160×160 grid at $Ra = 2.51 \times 10^{10}$.

Comparing the results for $0.25 \leqslant Pr \leqslant 2.0$ and $2.5 \leqslant Pr \leqslant 7.0$, it appears that the differences in the qualitative character of the transition from laminar to chaotic flow in the square cavity can be largely explained by a change in the nature of the boundary-layer instability for increasing Prandtl number. For $Pr \leqslant 2$, the boundary-layer oscillation is periodic in time, whereas for $Pr \geqslant 2.5$, the oscillation is chaotic (i.e. it has a broadband spectrum). Somewhere in the range $2 < Pr < 2.5$, the nature of the boundary-layer instability in the square cavity must change. This can also explain why such a large difference occurs between the cavity and the isolated vertical plate configuration, at least for Prandtl numbers larger than 2. For the vertical plate configuration, a selective frequency amplification mechanism was found (Gebhart *et al.* 1988). For the boundary-layer instability in the square cavity, this selective frequency amplification mechanism becomes weaker for increasing Prandtl number. This process is illustrated in figure 6(*a–c*) which shows the power spectra calculated from the temperature at the monitor point in the downstream part of the hot vertical boundary layer. Results are depicted for Prandtl numbers 0.71, 1.0 and 2.0 respectively, for Rayleigh numbers just above the critical Rayleigh number. The figures show clearly that for increasing Prandtl number the range of frequencies amplified in the frequency band $0.5\text{–}1.0(g\beta\Delta TH)^{1/2}/H$ increases and that the power in the frequencies, corresponding to linear combinations of the two fundamental frequencies, increases relative to the boundary-layer frequency. For higher values of the Prandtl number, spectra as depicted in figure 5(*b*) appear and no single boundary-layer frequency can be found anymore.

5.2. *Low-frequency instability*

Results obtained for the low-frequency oscillation in the square cavity after the bifurcation have been tabulated in table 2 for three of the different Prandtl numbers investigated. The table shows for these Prandtl numbers the frequency f_l of the low-frequency oscillation together with two values of the Rayleigh number, Ra_d and Ra_l. Here, Ra_d is the highest calculated value of the Rayleigh number at which the low-frequency oscillation was damped and Ra_l the lowest calculated value of the Rayleigh number at which the oscillation with frequency f_l was obtained in the solution for large time.

As can be seen from the results in table 2, the critical Rayleigh number increases

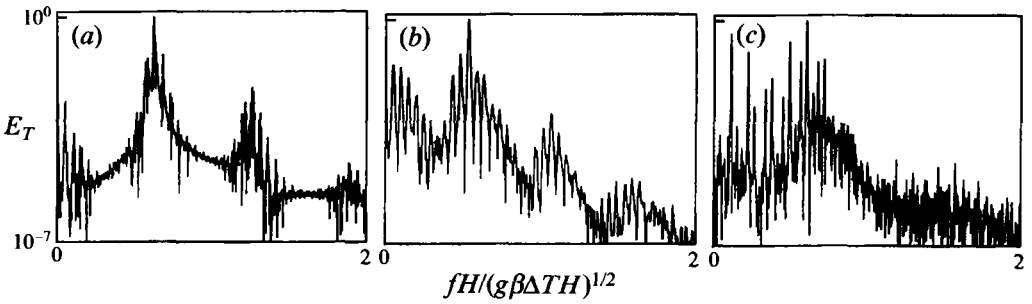

FIGURE 6. Power spectra of the temperature oscillation at the monitor point $(x/H, y/H) = (0.0025, 0.90)$ for three different values of the Prandtl number: (*a*) $Pr = 0.71$ at $Ra = 3 \times 10^8$, (*b*) $Pr = 1.0$ at $Ra = 5 \times 10^8$ and (*c*) $Pr = 2.0$ at $Ra = 5 \times 10^9$.

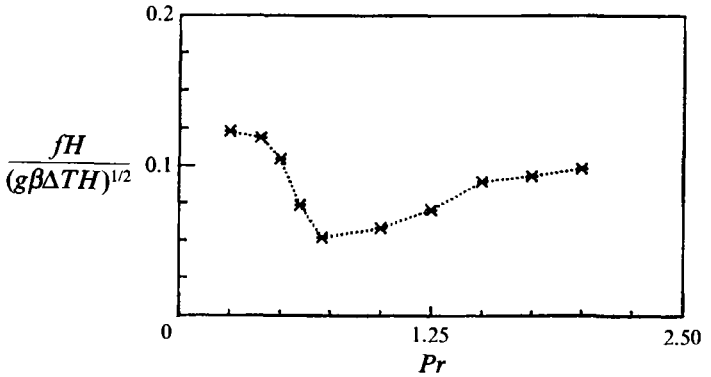

FIGURE 7. Frequency, f_l, of the low-frequency oscillation as a function of Prandtl number.

Pr	$\frac{f_l H}{(g\beta\Delta TH)^{1/2}}$	Ra_d	Ra_1
0.25	0.123	3.5×10^7	4.25×10^7
0.71	0.0522	1.5×10^8	2.0×10^8
2.0	0.0985	1.0×10^9	2.0×10^9

TABLE 2. Results for the low-frequency instability in the square cavity.

from approximately 4×10^7 for $Pr = 0.25$ to approximately 2×10^9 for $Pr = 2.0$. The dimensionless frequency of the oscillation changes by a factor of approximately 2 over the range of Prandtl number values considered here. In figure 7, the variation of the frequency f_l as a function of Prandtl number has been plotted for all calculated Prandtl number values in the range 0.25–2.0. The figure shows that there is a gradual decrease of the frequency as the Prandtl number is increased from 0.25 to 0.71 and then an even more gradual increase as the Prandtl number increases from 0.71 to 2.0. The fact that this change in frequency takes place gradually and is relatively small suggests that the instability mechanism is the same for all Prandtl numbers in the range 0.25–2.0.

To investigate the origin of the oscillation in the flow for the different Prandtl numbers and thus to determine whether the low-frequency oscillation is, for all

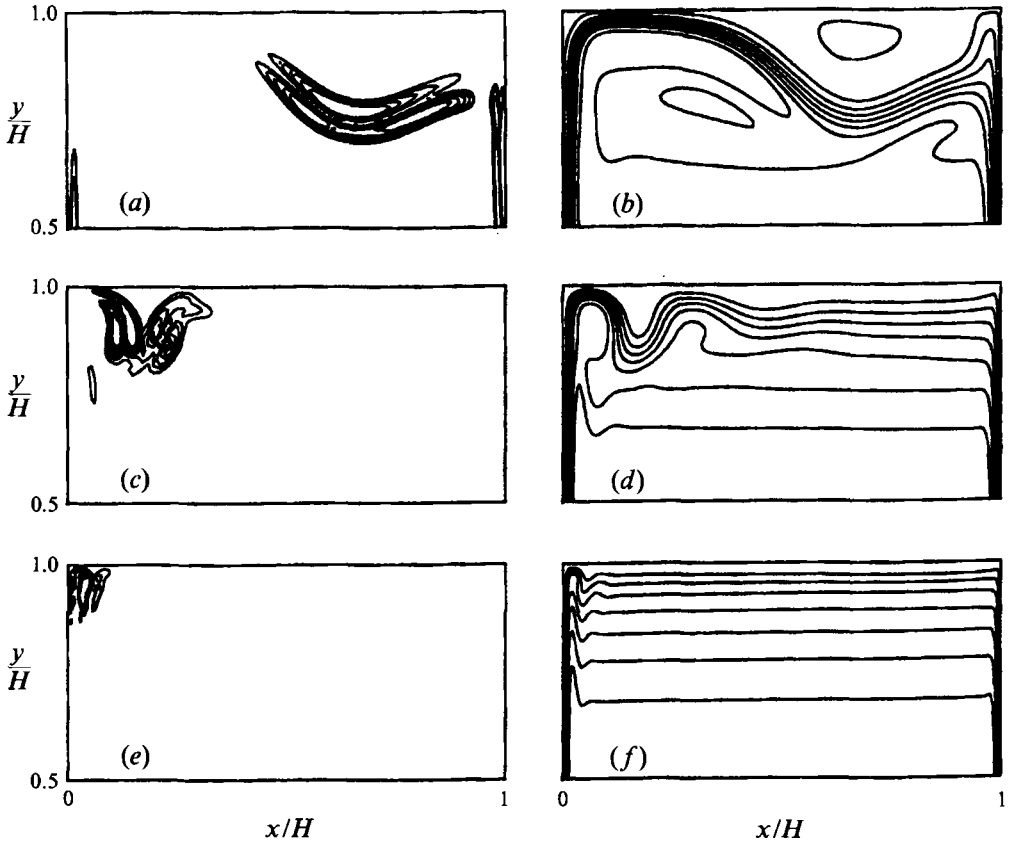

FIGURE 8. Amplitude of the oscillation in the kinetic energy (a, c, e) and time-averaged streamlines (b, d, f) in the upper half of the cavity. Contourlines for the amplitude correspond to 0.2, 0.3, 0.4, 0.5, 0.6 and 0.7 times the maximum value. The streamlines correspond to 7 equidistant values. (a, b) $Pr = 0.25$ and $Ra = 4.25 \times 10^7$, (c, d) $Pr = 0.71$ and $Ra = 2 \times 10^8$, (e, f) $Pr = 2$ and $Ra = 2 \times 10^9$.

these Prandtl numbers, caused by the same instability mechanism, amplitudes of the oscillation in the kinetic energy, together with time-averaged streamlines are depicted in figure 8(a–f). The amplitudes have been defined here as the difference between the maximum and the minimum value of the kinetic energy. The figure shows the upper half ($H/2 < y < H$) of the square cavity for Prandtl numbers 0.25, 0.71 and 2.0 respectively. The flow in the lower half of the cavity is symmetric with the flow in the upper half of the cavity. The figure demonstrates clearly the intimate connection between the flow divergence on the one hand, which originates from the upper left corner where the hot vertical boundary layer is turned horizontal by the presence of the adiabatic horizontal wall, and the oscillations on the other hand.

Ivey (1984) proposed that the flow divergence was an *internal* hydraulic-jump related to the hydraulic jump as it occurs in open channel flow. This proposition was supported by the work of Paolucci & Chenoweth (1989) who obtained a rather good agreement between the critical Rayleigh number they predicted using simplified hydraulic jump-theory and the actual occurrence of the bifurcation in their numerical calculations of the flow of air ($Pr = 0.71$) in cavities with aspect ratios between 0.5 and 3. However, this conjecture of an internal hydraulic jump has recently been questioned by Patterson & Armfield (1992) and by Ravi *et al.* (1994). Ravi *et al.*

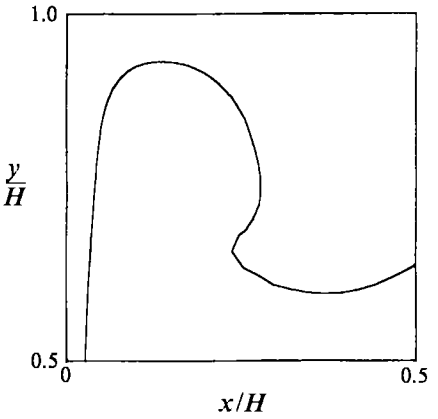

FIGURE 9. Isotherm $(T - T_c)/(T_h - T_c)$=0.80 for air ($Pr = 0.71$) at $Ra = 10^8$ in the upper left quarter of the cavity.

(1994) performed an elaborate and detailed investigation to determine whether or not a hydraulic jump did occur. They found that the behaviour of the flow divergence with varying Rayleigh number did not correspond at all to the behaviour that might be expected from hydraulic-jump theory. Also, it was found that there was no significant loss of mechanical energy associated with the flow expansion, as there is for a hydraulic jump. Thus, they concluded that the divergence was not a hydraulic jump but that it was basically caused by a thermal mechanism. The reasoning behind the mechanism they propose is displayed in figure 9. It shows the time-averaged isotherm $(T - T_c)/(T_h - T_c) = 0.80$ for air at $Ra = 2 \times 10^8$ in the upper left quarter of the cavity. As can be seen in figure 9, the y-level of the isotherm in the core region at $x = H/2$ is considerably below its level in the vicinity of the corner. The fact that the temperature of part of the fluid after turning the corner is lower than the temperature of the fluid in the core region at the same y-position causes the layer exiting from the corner to experience a (negative) buoyancy force, which forces it downward and the fluid layer enters the core region somewhat like an internal jet. This jet-like character is especially pronounced for low values of the Prandtl number (i.e. lower than 0.71, the value for air), since the stratification in the core region is largest for these low values of the Prandtl number, leading to the largest downward buoyant force.

To study more precisely the nature of the oscillations and their relation with the time-averaged jet-like flow structure, vorticity perturbations in the flow have been visualized. These were obtained by subtracting the local time-averaged values of the vorticity at every grid point from the instantaneous values at 40 time instants, distributed uniformly over one period of the oscillation. Four of the resulting pictures for $Pr = 0.25$ at $Ra = 4.25 \times 10^7$ distributed uniformly over one period of the oscillation are shown in figure 10. They show the vorticity fluctuations together with time-averaged streamlines. The two extreme streamlines demarcate approximately the boundaries of the fluid layer which exits from the upper left corner of the cavity. It is clear from figure 10 that the vorticity fluctuations occur in localized 'spots' (i.e. the vorticity fluctuations appear concentrated in small regions). As figure 10 shows these spots arise in and are carried with the mean flow in this layer forming a sort of vortex street. This suggests that the instability is basically of the Kelvin–Helmholtz type and is related to the presence of points of inflexion in the mean flow velocity distribution. Another point to be noted from figure 10 is that the vorticity perturbations arise

approximately symmetrically around the centreline of the jet-like fluid layer. In appearance at least, this is very similar to the distribution of vorticity perturbations in an inviscid, parallel plane Bickley jet, as can be derived from the analytical results documented in Drazin & Howard (1966) and from the numerical results of Comte, Lesieur & Chollet (1987).

The Bickley jet is the solution of the flow equations, obtained using the boundary-layer approximation, for the laminar flow issuing from a point source (Schlichting 1968). Its longitudinal velocity, assuming parallel flow also, is given by

$$u(y) = \frac{U_0}{\cosh^2(y/\delta_0)}, \tag{5.1}$$

where δ_0 is a suitably chosen transverse length scale. Stability results for the parallel Bickley jet show that the flow given by equation (5.1) is unstable for Reynolds numbers, $Re = U_0\delta_0/\nu$, larger than 4. The instability is a Kelvin–Helmholtz-type instability, driven by the shear stresses and related to the presence of two points of inflexion in the velocity distribution given in equation (5.1). These points of inflexion are located at

$$y = \pm 0.6585\delta_0. \tag{5.2}$$

The stability of the non-parallel Bickley jet has been studied numerically by Garg (1981). His results differ somewhat from the parallel flow results and suggest that the critical Reynolds number for the non-parallel Bickley jet is approximately 20. The frequencies, $f\delta_0/U_0$, which will be amplified are in the range between 0.010 and 0.065. Apart from showing a broad range of frequencies which will be amplified, Garg's results show that which frequency is amplified the most depends on the position inside the jet. His results suggest therefore that any frequency in this relatively broad range may be amplified and become dominant.

To check the assumed analogy between the Bickley jet and the cavity flow somewhat further, the time-averaged velocity distribution along the line which is indicated by the arrows in figure 10 has been calculated. This distribution is shown in figure 11. From this distribution, values of U_0 and δ_0 can be estimated (by taking the maximum value of the velocity and by determining the distance from the point of inflexion to the centreline of the jet and using equation (5.2)) and the theoretical Bickley jet profile obtained from these estimated values, using equation (5.1), is also displayed. It is clear that there is, at least approximately, similarity between the two velocity profiles. Using these values of U_0 and δ_0, the frequency $f\delta_0/U_0$ was found to be 0.04 for $Pr = 0.25$ and $Ra = 4.25 \times 10^7$. This value is in the range of frequencies that would have been expected from the Bickley jet results.

Typical distributions of the vorticity perturbations for $Pr = 0.71$ and $Pr = 2.0$ have been depicted in figures 12(*a*) and 12(*b*). These figures also show vorticity perturbations concentrated in localized regions, roughly aligned along the mean flow and symmetrical around the centre of the fluid layer. This suggests that the low-frequency instability is, for all Prandtl numbers under consideration, caused by a Kelvin–Helmholtz-type shear instability. The frequencies, $f\delta_0/U_0$, for $Pr = 0.71$ and $Pr = 2.0$ in the square cavity are 0.02 and 0.06 respectively and are therefore also in the range that is to be expected.

If the instability is indeed a Kelvin–Helmholtz-type instability and is furthermore related to the presence of inflexion points in the velocity profile, then the instability is basically of an inviscid type and it should therefore be expected that the instability disappears for small Reynolds numbers. Generally speaking (Schlichting 1968), it must

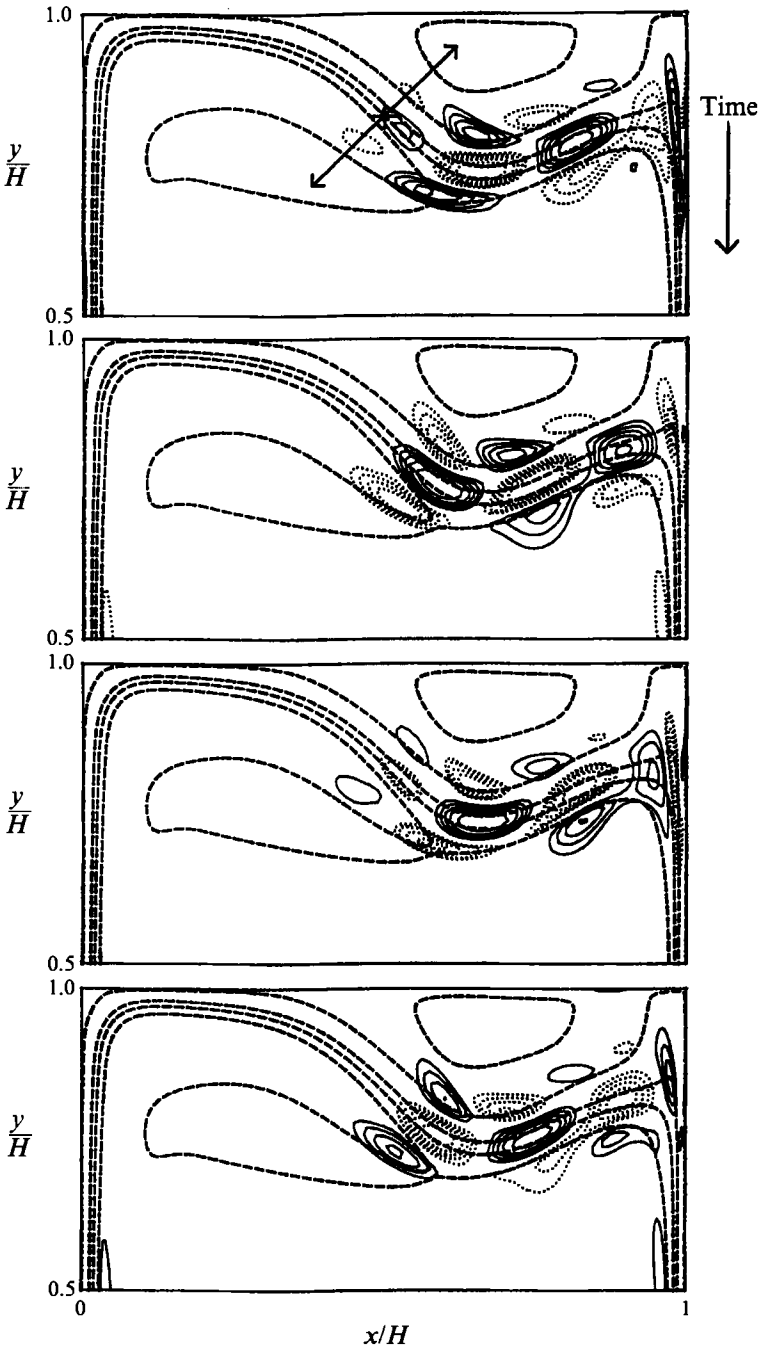

FIGURE 10. Vorticity perturbations and time-averaged streamlines (dashed contours) in the upper half of the square cavity for $Pr = 0.25$ and $Ra = 4.25 \times 10^7$. Dotted contour lines correspond to negative values. Vorticity contours for ± 0.15, ± 0.25, ± 0.35, ± 0.45, ± 0.6 $(g\beta\Delta T H)^{1/2}/H$ are shown. The + sign marks the position where the perturbations originate and the velocity profile in figure 11 is taken along the line indicated by the arrows.

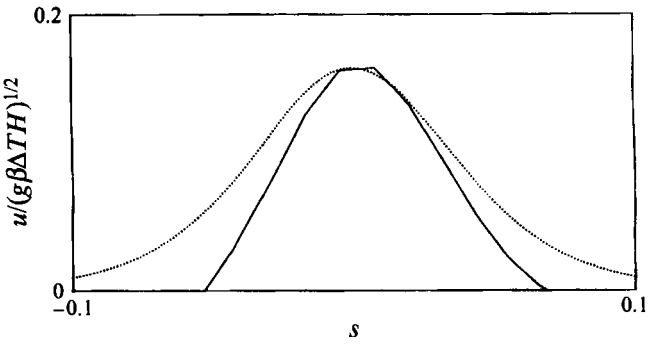

FIGURE 11. Theoretical velocity profile of the Bickley jet (dotted) and the calculated velocity profile in the cavity along the line indicated in figure 10. The value $s = 0$ corresponds to the location of the + sign in figure 10.

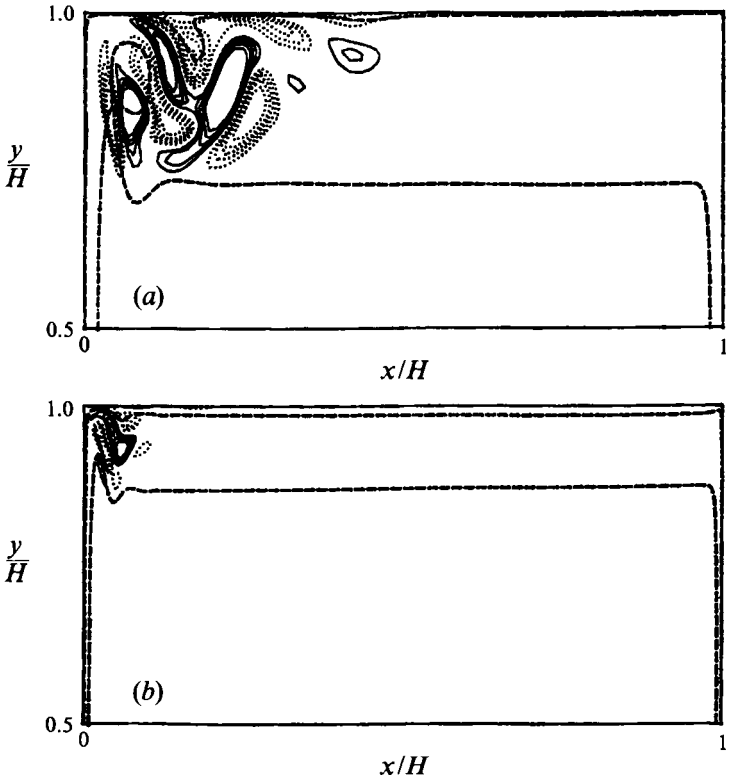

FIGURE 12. Vorticity perturbations and time-averaged streamlines in the upper half of the square cavity for $Pr = 0.71$ (*a*) and for $Pr = 2.0$ (*b*). The vorticity perturbations are for the same values as in figure 10.

be expected that values of the Reynolds number of the order of 20 are necessary to neglect viscosity in the treatment of a stability problem. The Reynolds-number values based on the length scale δ_0 and the velocity scale U_0 as determined from the time-averaged flow fields are tabulated in table 3. It can be seen that the Reynolds number of the jet-like fluid layer decreases from 99 for $Pr = 0.25$ to 25 for $Pr = 2.0$.

Pr	Re $(U_0\delta_0/\nu)$	$f_l\delta_0/U_0$	E_{shear} (%)	E_{buoy} (%)
0.25	99	0.04	100	−32
0.71	67	0.02	94	6
2.0	25	0.06	65	35

Bickley jet (Garg 1981)

Re_{cr} $(U_0\delta_0/\nu)$	$f\delta_0/U_0$
22	0.01 – 0.065

TABLE 3. Results for the low-frequency instability in the square cavity and for the non-parallel Bickley jet. The last two columns give the production of fluctuating kinetic energy by shear and buoyancy forces.

Hence, for the Prandtl numbers in the range $0.25 \leqslant Pr \leqslant 2.0$, the Reynolds numbers seem large enough for an essentially inviscid instability to occur.

As a final check for the proposed instability mechanism, the balance of the fluctuating kinetic energy, as given by equation (2.4) has been calculated, by integrating all terms in group III over one period of the oscillation and over the entire cavity. If the instability is related to the presence of points of inflexion in the fluid layer, it is expected that the main contribution to the production of fluctuating kinetic energy is given by the shear stress term $-\overline{u_i'u_j'}\partial\overline{u}_i/\partial x_j$. The results for $Pr = 0.25$, 0.71 and 2.0 are also given in table 3. They show that indeed in all instances the shear stresses are the main contributors to the production of fluctuating kinetic energy. For $Pr = 0.25$, the buoyancy even contributes negatively to the production of fluctuating kinetic energy.

5.3. *Boundary-layer instability*

For $0.25 \leqslant Pr \leqslant 2.0$, increasing the Rayleigh number of the flow in the square cavity far enough leads to the occurrence of another, higher, fundamental frequency, f_h, in the flow. The critical Rayleigh number at which this occurs will be denoted as $Ra_{cr,h}$. The calculations prove that this second fundamental frequency is present only in quantities located in or near the boundary layers along the vertical walls. To show this, the spatial dependence of the power spectral density was calculated, i.e. the squared magnitude of the Fourier-component $\hat{T}(x, y, f^*)$ was calculated for $f^* = f_h$. Here, $\hat{T}(x, y, f^*)$ is given by

$$\hat{T}(x, y, f^*) = \int T(x, y, t)\mathrm{e}^{-\mathrm{i}(2\pi f^* t)}\mathrm{d}t, \tag{5.3}$$

in which i denotes the imaginary unit. The result for air ($Pr = 0.71$) at $Ra = 3 \times 10^8$ in the square cavity is shown in figure 13. The integration in time in equation (5.3) has been performed over approximately 80 periods of the high-frequency oscillation to obtain a good accuracy for the calculated power spectrum. Figure 13 shows that the oscillations are especially strong in the downstream part of the vertical boundary layers.

The form which this high-frequency instability takes is shown in figure 14 (again for $Pr = 0.71$ and $Ra = 3 \times 10^8$). Here, the temperature perturbations in the vertical boundary layer along the hot cavity wall have been visualized by subtracting the time-averaged temperature at every grid point from the instantaneous values at the instants shown (note that only 1/40th of the cavity is depicted in figure 14). Time averaging was performed over one period of the high-frequency oscillation. Also shown are the

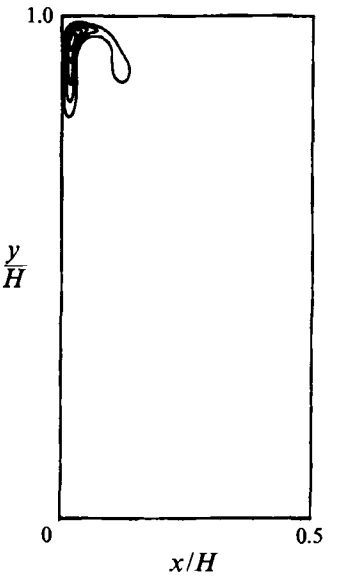

FIGURE 13. Spatial dependence of the power spectral density ($|\hat{T}(x, y, f^*)|^2$) for air ($Pr = 0.71$) at $Ra = 3 \times 10^8$. Here, the frequency f^* is taken equal to $0.6309(g\beta\Delta TH)^{1/2}/H$. Contour lines correspond to 0.1, 0.3, 0.5, 0.7 and 0.9 times the maximum value.

zero-perturbation lines (corresponding to locations where the instantaneous values are equal to the time-averaged values). Figure 14 shows that the perturbations have the character of a travelling wave in the vertical boundary layer.

In the past, this high-frequency instability for air has been attributed to an instability in the vertical boundary layers and has been compared to the boundary-layer instability, occurring in the natural-convection boundary layer along a semi-infinite vertical plate in a stratified environment (Le Quéré & Alziary de Roquefort 1985; Paolucci & Chenoweth 1989). Paolucci & Chenoweth (1989) obtained a reasonable agreement for air between the critical Rayleigh number predicted by equation (4.4), substituting the result of Gill & Davey (1969) for R_{GD} and their own stratification value S (= 1.0) calculated for the cavity, and the actual critical Rayleigh number observed for the high-frequency instability. When we compare our results for air in the square cavity we can draw the same conclusion with an estimated critical Rayleigh number of 1.1×10^8 according to equation (4.4) compared to an actually observed critical Rayleigh number between 2.5×10^8 and 3.0×10^8. However, for higher values of the Prandtl number, large discrepancies between the two configurations occur: in the square cavity for $Pr = 2.0$ we find $4 \times 10^9 < Ra_{cr,h} < 5 \times 10^9$. This is approximately two orders of magnitude larger than the critical Rayleigh number (3.63×10^7) estimated from equation (4.4) substituting the critical Reynolds number, R_{GD}, calculated by Gill & Davey and the stratification value S (= 0.65) we find in our calculations for the square cavity. This makes the assumed analogy rather questionable. It is interesting to note that Nachtsheim (1963), who performed a linear stability analysis for the natural-convection boundary layer along a hot *isothermal* plate, placed in an *isothermal* environment, had already noticed that the critical Rayleigh number he obtained for air was several orders of magnitude lower than that obtained in experiments.

In both the studies of Nachtsheim (1963) and Gill & Davey (1969), it was found that these instabilities, with their low critical Rayleigh number, corresponded to

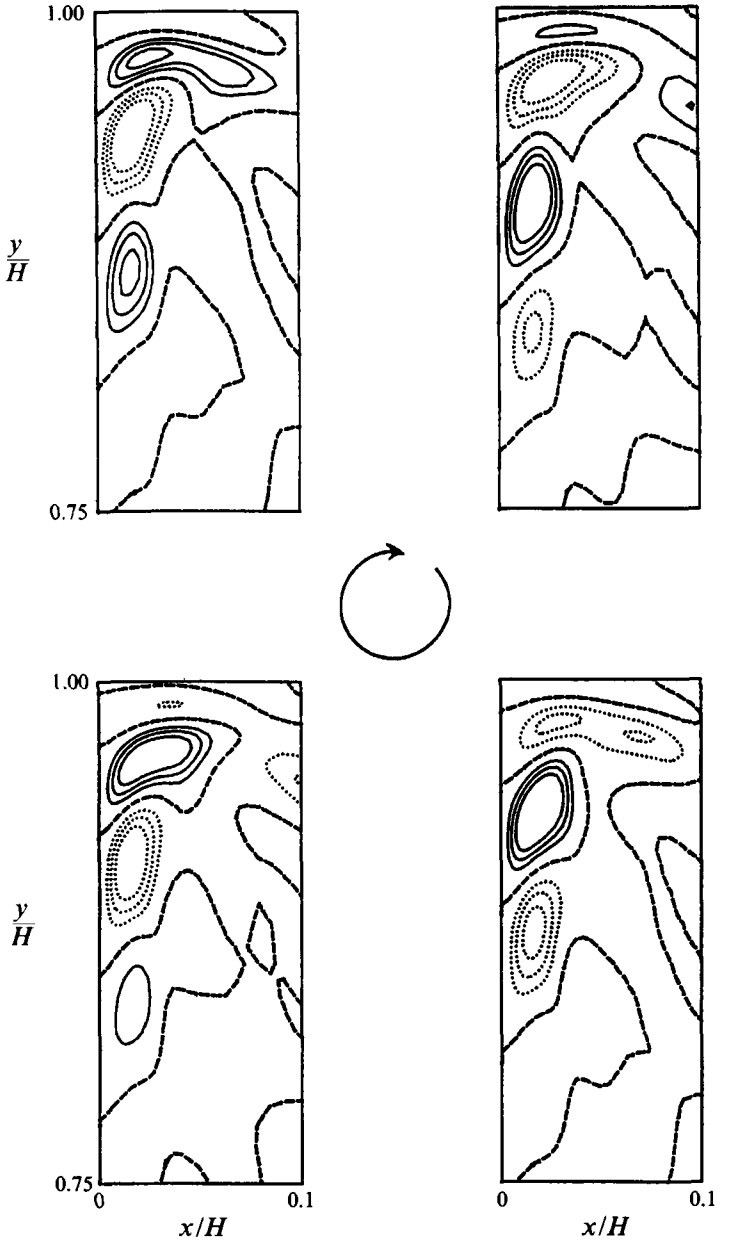

FIGURE 14. Temperature perturbations corresponding to the boundary-layer instability in the downstream part of the vertical boundary layer along the hot wall in the square cavity for air at $Ra = 3 \times 10^8$. Only that part of the cavity for which $0 < x/H < 0.1$ and $0.75 < y/H < 1.0$ is shown. The dotted contour lines correspond to negative values. Contour lines correspond to ± 0.016, ± 0.012 and ± 0.008 ΔT. The dashed lines correspond to zero-perturbation contour lines. The plots are a quarter of the period of the boundary-layer instability apart.

instabilities which were buoyancy-driven, i.e. the temperature fluctuations were the main contributors to the production of fluctuating kinetic energy. Gill & Davey (1969) actually calculated two types of instability for the vertical plate configuration: a low-wavenumber and a high-wavenumber instability. The low-wavenumber instability

Square cavity

Pr	Ra_d	Ra_2	$\frac{f\nu^{1/3}}{(g\beta\Delta T)^{2/3}}$
0.71	2.5×10^8	3.0×10^8	0.0230
1.0	2.0×10^8	5.0×10^8	0.0190
2.0	4.0×10^9	5.0×10^9	0.0159

Vertical plate; shear instability

Pr	Ra_{cr}	$\frac{f\nu^{1/3}}{(g\beta\Delta T)^{2/3}}$
0.72	1.52×10^8	0.0303
1.0	4.60×10^8	0.0323
2.0	4.57×10^9	0.0338

TABLE 4. Results for the boundary-layer instability.

had the lowest critical Rayleigh number and was mainly buoyancy-driven. The high-wavenumber instability was mainly shear-driven. If we compare the critical Rayleigh numbers obtained in the square cavity with those of Gill & Davey for the shear-driven instability along the isolated vertical plate, a quite good agreement is obtained, as is evident from table 4. The critical Rayleigh numbers agree within a factor of 2 with each other.

To check whether the disturbance in the cavity geometry is either buoyancy- or shear-driven, equation (2.4) needs to be integrated over the entire cavity and one period of the oscillation. However, in the *square* cavity, for the Prandtl numbers under consideration here, the high-frequency instability has a higher critical Rayleigh number than the low-frequency instability associated with the internal jet. Furthermore, the low-frequency oscillations are far more energetic than the high-frequency oscillations so it is difficult to determine the energy contributions of shear and buoyancy for the boundary-layer instability with sufficient accuracy. For higher values of the aspect ratio ($A > 3$), the low-frequency oscillation is absent (see Le Quéré & Alziary de Roquefort 1985). Hence, energy calculations were performed for the cavity with aspect ratio 4 (for this aspect ratio the two vertical boundary layers are still well separated as is the case in the square cavity). For the cavity with aspect ratio 4 at $Ra = 1.2 \times 10^8$, integration of the energy equation (2.4) showed that the contribution of the shear terms to the production of the fluctuating kinetic energy was approximately 95% of the total production, which supports the previously proposed explanation for the observed critical Rayleigh numbers.

The frequencies obtained are $0.0206(g\beta\Delta T)^{2/3}\nu^{-1/3}$ for the cavity with aspect ratio 4 and $0.0230(g\beta\Delta T)^{2/3}\nu^{-1/3}$ for the square cavity. These values differ by 50% and 30% respectively from the value $0.0303(g\beta\Delta T)^{2/3}\nu^{-1/3}$ obtained by Gill & Davey (1969) for the boundary layer along the vertical plate. To the same extent, Paolucci & Chenoweth (1989) and Le Quéré & Alziary de Roquefort (1985) obtained agreement between their results for the frequency of the boundary-layer instability for air in the cavity for different values of the aspect ratio and the results of Gill & Davey (1969) for the vertical plate. The difference between the two configurations as far as the frequencies are concerned becomes more pronounced as the Prandtl number increases (for $Pr = 2$ in the square cavity $f_h = 0.0159(g\beta\Delta T)^{2/3}\nu^{-1/3}$ whereas for the

plate $0.0338(g\beta\Delta T)^{2/3}\nu^{-1/3}$). In view of the results described in §5.1 regarding the transition to a chaotic flow, this is not very surprising.

6. Conclusions

The work described in this paper examined the Prandtl-number dependence of the laminar–turbulent transition in a natural-convection flow inside a differentially heated, square cavity with adiabatic horizontal walls. It was found that for Prandtl numbers between 0.25 and 2.0, the transition took place through intermediate periodic and quasi-periodic flow regimes in agreement with the proposition made by Ruelle & Takens (1971). However, for Prandtl numbers between 2.5 and 7.0, no such intermediate regimes were found. Instead, a very small increase in Rayleigh number resulted in the flow going from steady to chaotic (where the term chaotic denotes a flow regime in which power spectra have no true dominant spikes and show clear broadband components). This difference between the two regimes is caused by a difference in the nature of the instability occurring in the vertical boundary layers.

For Prandtl numbers between 0.25 and 2.0, the instability which caused the transition from the steady to the periodic flow regime occurred in the jet-like fluid layer exiting from the upper left and lower right corners of the cavity. The disturbance received its energy mainly from the shear stresses exerted by the mean flow. The visualization of the vorticity perturbations showed that they were concentrated in small regions and were distributed approximately symmetrically around the centre of the jet-like fluid layer showing a close similarity to the vorticity distribution in a plane Bickley jet. This suggests that the instability is, as for the Bickley jet, an inviscid Kelvin–Helmholtz-type instability related to the presence of points of inflexion in the mean velocity profile. Also, if frequencies are compared, it is found that they are in or very near the range of unstable frequencies found for the Bickley jet. Furthermore, it is found that the local Reynolds numbers for the jet-like fluid layer decrease from approximately 99 for $Pr = 0.25$ to 25 for $Pr = 2.0$, giving further support to the suggestion that this instability is a Kelvin–Helmholtz-type instability related to the presence of points of inflexion in the mean velocity profile. The second bifurcation from the periodic to the quasi-periodic flow regime originates in the boundary layers along the vertical cavity walls. Previous investigations performed for *air* (Le Quéré & Alziary de Roquefort 1985; Paolucci & Chenoweth 1989) compared this instability with the instability occurring in the natural-convection boundary layer along an isolated vertical plate and obtained reasonable agreement. The present calculations also support this agreement for air ($Pr = 0.71$) but show that there is substantial disagreement between the two configurations for higher Prandtl numbers. It is found that these discrepancies can be largely resolved if it is assumed that the instability in the cavity is mainly shear-driven instead of it being buoyancy-driven like the instability occurring in the vertical plate configuration (Gill & Davey 1969).

The authors gratefully acknowledge the financial support from the foundation for 'Fundamental Research of Matter' (FOM) and the 'Royal Netherlands Academy of Arts and Sciences' (KNAW).

REFERENCES

Blythe, P. A., Daniels, P. G. & Simpkins, P. G. 1983 Thermal convection in a cavity: the core structure near the horizontal boundaries. *Proc. R. Soc. Lond.* A **387**, 367–388.

COMTE, P., LESIEUR, M. & CHOLLET, J. P. 1987 Simulation numérique d'un jet plan turbulent. *C.R. Acad. Sci. Paris* **305** Série II, 1037–1044.

DE VAHL DAVIS, G. & JONES, I. P. 1983 Natural-convection of air in a square cavity. *Intl J. Num. Meth. Fluids* **3**, 229–248.

DRAZIN, P. G. & HOWARD, L. N. 1966 Hydrodynamic stability of parallel flow of inviscid fluid. *Adv. Appl. Mech.* **9**, 1–89.

DRAZIN, P. G. & REID, W. H. 1981 *Hydrodynamic Stability*. Cambridge University Press.

ELDER, J. W. 1965 Laminar free convection in a vertical slot. *J. Fluid Mech.* **23**, 77–97.

GARG, V. K. 1981 Spatial stability of the non-parallel Bickley jet. *J. Fluid Mech.* **102**, 127–140.

GEBHART, B., JALURIA, Y., MAHAJAN, R. L. AND SAMMAKIA, B. 1988 *Buoyancy-Induced Flows and Transport*. Hemisphere Publishing Corporation.

GEBHART, B. & MAHAJAN, R. 1975 Characteristic disturbance frequency in vertical natural convection flow. *Intl J. Heat Mass Transfer* **18**, 1143–1148.

GILL, A. E. 1966 The boundary-layer regime for convection in a rectangular cavity. *J. Fluid Mech.* **26**, 515–536.

GILL, A. E. & DAVEY, A. 1969 Instabilities of a buoyancy-driven system. *J. Fluid Mech.* **35**, 775–798.

GRAEBEL, W. P. 1981 The influence of Prandtl number on free convection in a rectangular cavity. *Intl J. Heat Mass Transfer* **24**, 125–131.

HENKES, R. A. W. M. 1990 Natural-convection boundary layers. PhD thesis, Delft University of Technology.

HENKES, R. A. W. M. & HOOGENDOORN, C. J. 1993 Scaling of the laminar natural-convection flow in a heated square cavity. *Intl J. Heat Mass Transfer* **36**, 2913-2925.

IVEY, G. N. 1984 Experiments on transient natural convection in a cavity. *J. Fluid Mech.* **144**, 389–401.

JANSSEN. R. J. A. & HENKES, R. A. W. M. 1993 Accuracy of the finite-volume discretization for the bifurcating natural-convection flow in a heated square cavity. *Numer. Heat Transfer* B **24**, 191-207.

LE QUÉRÉ, P. & ALZIARY DE ROQUEFORT, T. 1985 Transition to unsteady natural convection of air in differentially heated vertical cavities. *4th Intl Conf. Num. Meth. in Laminar and Turbulent Flow*, pp. 841–852. Pineridge Press.

LE QUÉRÉ, P. & ALZIARY DE ROQUEFORT, T. 1986 Transition to unsteady natural convection of air in differentially heated vertical cavities: influence of thermal boundary condition on the horizontal walls. *Proc. 8th Intl Heat Transfer Conf.*, San Francisco, pp. 1533–1538.

MEIJERINK, J. A. & VAN DER VORST, H. A. 1977 An iterative solution method for linear systems of which the coefficient matrix is a symmetric M-matrix. *Math. Comput.* **31**, 148–162.

NACHTSHEIM, P. R. 1963 Stability of free-convection boundary-layer flows. *NASA TN* D-2089.

PAOLUCCI, S. & CHENOWETH, D. R. 1989 Transition to chaos in a differentially heated vertical cavity. *J. Fluid Mech.* **201**, 379–410.

PATTERSON, J. C. & ARMFIELD, S. W. 1992 Transient features of natural convection in a cavity. *J. Fluid Mech.* **219**, 469–498.

PATTERSON, J. C. & IMBERGER, J. 1980 Unsteady natural convection in a square cavity. *J. Fluid Mech.* **100**, 65–86.

RAVI, M. R., HENKES, R. A. W. M. & HOOGENDOORN, C. J. 1994 On the high Rayleigh number structure of steady laminar natural-convection flow in a square enclosure. *J. Fluid Mech.* **262**, 325-351.

RUELLE, D. & TAKENS, F. 1971 On the nature of turbulence. *Commun. Math. Phys.* **20**, 167–192.

SCHLADOW, S. G. 1990 Oscillatory motion in a side-heated cavity. *J. Fluid Mech.* **213**, 589–610.

SCHLADOW, S. G., PATTERSON, J. C. & STREET, R. L. 1989 Transient flow in a side-heated cavity at high Rayleigh number: a numerical study. *J. Fluid Mech.* **200**, 121–148.

SCHLICHTING, H. 1968 *Boundary-Layer Theory*. McGraw-Hill.

THORPE, S. A. 1968 On standing internal gravity waves of finite amplitude. *J. Fluid Mech.* **32**, 489–528.

TURNER, J. S. 1973 *Buoyancy Effects in Fluids*. Cambridge University Press.

VAN DER VORST, H. A. 1989 High performance preconditioning. *SIAM J. Sci. Stat. Comput.* **10**, 1174–1185.

WINTERS, K. H. 1987 Hopf bifurcation in the double-glazing problem with conducting boundaries. *J. Heat Transfer* **109**, 894–898.

WINTERS, K. H. 1988 Oscillatory convection in liquid metals in a horizontal temperature gradient. *Intl J. Numer. Methods Engng* **25**, 401–414.

WINTERS, K. H. 1989 A bifurcation analysis of oscillatory convection in liquid metals. *Proc. Gamm-Workshop on Numerical Simulation of Oscillatory Convection in Low Pr Fluids*, pp. 319–326. Vieweg.